Journal of Alloys and Compounds 930 (2023) 167409

Contents lists available at ScienceDirect

Journal of Alloys and Compounds

journal homepage: www.elsevier.com/locate/jalcom

$Ge_{1-x}S_x$ chalcogenide alloys for OTS applications using magnetron sputtering

Minkyu Lee [a,1], Sanghyeon Lee [b,1], Myoungsub Kim [a,d], Seungmin Lee [a], Chihyeong Won [a], Taehoon Kim [d], Chaebeen Kwon [a], Kukro Yoon [a], Jinhan Lee [a], Hyungjun Kim [a], Taeyoon Lee [a,c,*]

[a] School of Electrical and Electronic Engineering, Yonsei University, Seoul 03722, South Korea
[b] KIURI Institute, Yonsei University, Seoul 03722, South Korea
[c] Department of Bio and Brain Engineering, Korea Institute of Science and Technology (KIST), 5 Hwarang-ro 14-gil, Seongbuk-gu, Seoul 02792, South Korea
[d] SK Hynix, 2091, Gyeongchung-daero, Bubal-eup, Icheon-si, Gyeonggi-do, South Korea

ARTICLE INFO

Article history:
Received 11 July 2022
Received in revised form 24 September 2022
Accepted 28 September 2022
Available online 30 September 2022

Keywords:
Germanium
Sulfur
Chalcogenide
OTS selector
Magnetron Sputtering
Cross–point memory

ABSTRACT

3D cross (X)–point memory arrays have attracted attention for future memory architecture due to their cost efficiency and high density. Chalcogenide–based materials are suitable candidates for 3D X–point memory because they can be stacked to form both memory and selector with a simple process. Conventional binary chalcogenide ovonic threshold switching (OTS) selectors such as Ge_XSe_{1-x} or GeTe suffer from thermal instability. Furthermore, ternary OTS selectors are being investigated by doping various materials to overcome thermal instability. Here, we introduce a wide range of $Ge_{1-x}S_x$ films to analyze and confirm the selector behavior for future applications. S–rich region ($0.5 \le x \le 0.67$) devices behaved as OTS selector with low leakage current (1.3 nA) and high thermal stability (amorphous up to 600 °C). To study the mechanism of devices with different compositions, the modified PF–model was used to calculate trap density, activation energy, subthreshold swing, and distance between traps. Additionally, extracted optical bandgap (1.65 – 3.45 eV) and urbach energy (166 – 103 meV) had good accordance with electrical characteristics of each device. This innovative research has potential to enable 3D X–point memory by combining conformal OTS selector and chalcogenide–based phase change memory.

1. Introduction

Due to emerging technologies such as big data, cloud computing, and neuromorphic computing, memory products have required fast access speed, high density, and low power consumption [1–3]. Chalcogenide–based phase–change random access memory (PCRAM), a candidate that meets those requirements, has been investigated and commercialized [4–6]. Three–dimensional (3D) cross–point (X–point) memory devices have attracted attention as new memory array architecture due to their high storage density [7–10]. However, the 3D stacking array has suffered from sneak path current, causing the cross–talk interference between adjacent cells, which can lead to misinterpretation [11]. It is very beneficial that PCRAM is coupled with a selector device vertically to minimize cell–to–cell interference and maximize memory density [12–15]. Chalcogenide Ovonic Threshold Switching (OTS) selectors are the most suitable candidate because of the rapid and reliable reversible transition between high resistive (OFF state) and conductive (ON state) by subtle atomic rearrangements under an applied critical electric field E_{th} (or threshold voltage V_{th}) without phase change in an amorphous state.

Several studies on binary chalcogenide OTS selectors based on either Te or Se alloys combined with Ge have been reported [16–19]. Anbarasu et al. fabricated $GeTe_6$–based OTS device, which shows fast threshold switching (5 ns) and stability of the on/off state over 600 cycles [20]. Song et al. demonstrated a $Ge_{1-x}Se_x$ OTS device, which has improved performance, such as low leakage current at off state (I_{off} < 0.1 nA at 1/2 V_{th} of 1 V), high current at the on state (I_{on} > 1 mA at V_{th} of 2 V), and sharp switching slope (< 3 mV/dec) [21]. However, those binary OTS selectors are thermally unstable and have a low thermal budget due to crystallization or segregation from glassy

* Corresponding author at: School of Electrical and Electronic Engineering, Yonsei University, Seoul 03722, South Korea.
E-mail address: taeyoon.lee@yonsei.ac.kr (T. Lee).
[1] Minkyu Lee and Sanghyeon Lee equally contributed to this work

https://doi.org/10.1016/j.jallcom.2022.167409
0925-8388/

structures [22]. To enhance thermal stability, ternary OTS selectors are fabricated by doping or incorporating materials including As, N, and Sb [23]. Liu et al. implanted As ions into sputtered GeSe layers, which maintained an amorphous phase even at elevated temperature (400 °C) and had a high I_{on} of 10 mA at 2.5 V [24]. Those conventional chalcogenide OTS selectors still suffer from toxicity and complexity. Thus, thermally stable OTS selectors with simple processes and outstanding performance are strongly demanded.

Recently, $Ge_{1-x}S_x$ alloy films have emerged as a replacement for conventional OTS selector devices due to their high thermal stability and large optical bandgap [25,26]. In terms of atomic bonding, OTS selectors are preferable because they have stronger covalent bonding, which improves thermal stability and results in a high I_{on} [27,28]. Thus, lighter and smaller S elements compared to those of Se and Te may lead to stronger covalent bonds by increasing the hybridization of $Ge_{1-x}S_x$ alloy films [29]. Furthermore, I_{off} and larger selectivity (I_{on}/I_{off}) can be expected due to the larger optical bandgap of $Ge_{1-x}S_x$ than those of GeTe and $Ge_{1-x}Se_x$ [30–34]. Despite of being appealing material, systematic studies for wide range of $Ge_{1-x}S_x$ alloy films have not been reported.

In this study, we analyzed a wide range of S compositions in $Ge_{1-x}S_x$ alloy layers to better understand OTS behavior, thermal stability, AC/DC transient characteristics, and optical properties. To investigate the device behavior of a selector, the device was fabricated with a Ru/Amorphous–C/$Ge_{1-x}S_x$/TiN structure. Each part plays the role of the top electrode, insulating layer, OTS selector, and bottom electrode, respectively. The device demonstrated different transient characteristics with variations in the Ge and S ratio. Devices with Ge–rich composition ($0.2 \le x < 0.5$) showed metallic behavior after applying electrical fields. In as–deposited state, the film remained in an amorphous state, which consists of some broken covalent bonds along with lone pairs or vacancies. After joule heating induced from the electric field, Ge atoms occupied vacancy sites and recombined with lone pairs, which led to the crystallization of films. On the other hand, the device with S–rich compositions ($0.5 \le x \le 0.67$) demonstrated reliable OTS behavior with high electrical performance and thermal stability. *In–situ* X–ray Diffraction analysis (XRD) confirmed that the films remained as an amorphous state from as–deposited to 600 °C. In DC–IV characteristics, the V_{th} increased from 3.4 to 5.0 V and I_{off} decreased from 20 to 1.3 nA as the S composition increased. Activation energies (E_a) and trap densities (N_t) increased from 518 to 630 meV, and 3.14×10^{20} to 4.83×10^{20} cm^{-3}, respectively, of which values were calculated using the modified Poole–Frenkel (PF) model. Fast on/off switching speeds up to 15 ns (t_{on}) and 20 ns (t_{off}) were observed in AC I–V characteristics, with high stability (~ 10^9 cycles). Optical properties had good accordance with the electrical characteristics; the higher the optical bandgap, the higher V_{th}.

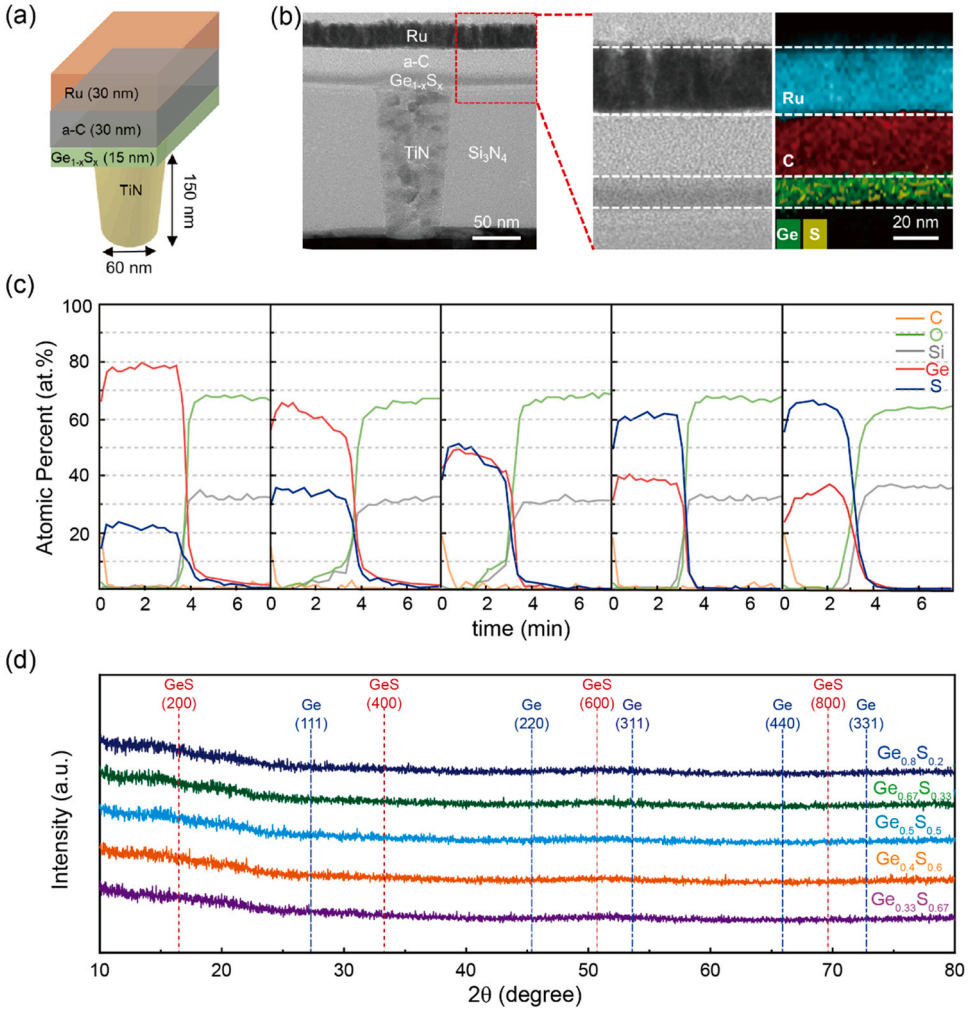

Fig. 1. (a) Schematic of OTS device, (b) Cross–sectional TEM image of selector device based on $Ge_{1-x}S_x$ film and EDS mappings of each material, Ru (TE), a–C (insulator layer), Ge and S (selector layer). (c) Auger Electron Spectroscopy (AES) analysis of $Ge_{1-x}S_x$ film. (d) X–ray diffraction (XRD) curve of each composition at deposited.

2. Material and methods

2.1. Sample preparation

RF magnetron sputtering (SNTEK Co., LTD) was used to deposit $Ge_{1-x}S_x$ films using a $Ge_{0.33}S_{0.67}$ alloy target and germanium target, purchased from AVENTION (2inch diameter, 3 mm–thick). Under base pressure lower than $6E^{-6}$ Torr, the working pressure was set to 3 mTorr with Ar of 15 sccm, and the substrate temperature was set to 50 °C. $Ge_{1-x}S_x$ films were deposited through co–sputtering of the $Ge_{0.33}S_{0.67}$ alloy target and Ge target. The $Ge_{0.33}S_{0.67}$ plasma power was fixed at 50 W to prevent melting or segregation of the target, and Ge plasma power was adjusted from 5 ~ 25 W to confirm various compositions. A 100–nm–thick $SiO_2/Si(P^+)$ wafer was employed for the substrate.

2.2. Film analysis and electrical measurements

A scanning electron microscope (FEI, Nova Nano SEM 200) and transmission electron microscopy (TEM, JEOL, JEM F–200) were employed to measure the film thicknesses. Quantitate ratios of Ge, S, and impurity levels were analyzed using auger electron spectroscopy (AES, ULVAC, PHI–710). *In–situ* high–temperature XRD (HT–XRD, Rigaku, SmartLab) was employed to determine the thermal stability of each film. To measure the DC electrical characteristics, a Keithley 4200A–SCS semiconductor parameter analyzer was employed. Devices were fabricated by sputtering a–C (barrier layer) and Ru top electrode on top of $Ge_{1-x}S_x$ films using patterned mushroom–type 60–nm diameter TiN bottom electrode. Similarly, AC characteristics were measured by adding external phase measurement unit sensors.

2.3. Optical measurements

A UV/VIS–spectrophotometer (UV–VIS–NIR, Agilent, Cary5000) was used to measure the optical characteristics. The reflectance and transmittance of each composition were measured to calculate the optical bandgap. On quartz substrates, thicknesses were fixed at 500 nm, and reflectance and transmittance were measured with wavelengths ranging from 200 to 2000 nm.

3. Results and discussion

3.1. Growth of germanium sulfide film

Fig. 1a demonstrates the schematic of OTS selector devices. Using a patterned mushroom–type–60 nm diameter bottom electrode (TiN), $Ge_{1-x}S_x$ layers ($0.2 \le x \le 0.67$) were deposited with the same thickness of 15 nm using co–sputtering system. Fig. 1b shows the cross–sectional transmission image of the fabricated $Ge_{1-x}S_x$ selector device with an insulating layer (amorphous carbon (α–C)) and top electrode (Ru), of which thicknesses are 30 nm, respectively. Fig. 1b right–hand side transmission electron microscopy (TEM) and energy dispersive spectroscopy (EDS) elemental mapping images, which are magnified as red dotted areas of TEM image, exhibited clear and sharp interfaces. The α–C insulating layer was deposited on top of $Ge_{1-x}S_x$ layer to prevent an overflow of heat on the $Ge_{1-x}S_x$ layer, which improved the reliability of the selector device [35–37]. To test the reliability of devices, nine same–dimensional devices with/without α–C layers were fabricated. Devices without α–C layer showed unsteady variability (V_{th} of 4.8 ± 0.9 V), whereas devices with α–C layer demonstrated sharp distribution (V_{th} of 4.8 ± 0.1 V). The large variability shown in Fig. S1a can be attributed to the lack of a thermal insulator, which increased resistance in series. Compositional analyses were performed by AES using separately prepared $Ge_{1-x}S_x$ films deposited on 100–nm–thick $SiO_2/Si(P^+)$ substrates. Fig. 1c shows that the film compositions were uniform with a low level of impurities. The total amount of impurities only on the film was less than 3% throughout the film. As the plasma power of the Ge target was decreased, Ge contents in $Ge_{1-x}S_x$ layers decreased from 0.8 to 0.33. Fig. 1d illustrates the XRD patterns of as–deposited (~ 50 nm–thick) of $Ge_{1-x}S_x$ films, of which films were amorphous state regardless of compositional ratio. Deposited $Ge_{1-x}S_x$ films primarily

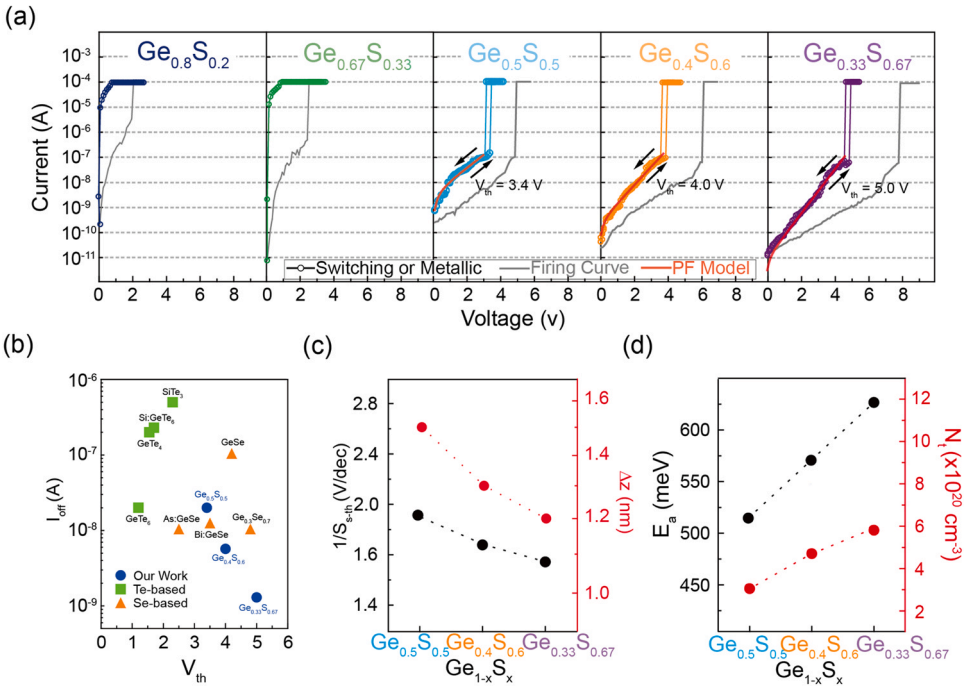

Fig. 2. (a) DC I–V characteristics of selector devices of $Ge_{1-x}S_x$ with thicknesses of 15 nm. Ge–rich composition ($0.2 \le x < 0.5$) devices exhibited metallic behavior, where S–rich composition ($0.5 \le x \le 0.67$) devices behaved as OTS selector. (b) Comparison of threshold voltage (V_{th}) and off current (I_{off}) from DC I–V curve with other works [43–46]. (c) Subthreshold slope ($1/S_{s\text{-}th}$) and distance between traps (Δz) of S–rich composition, where subthreshold slope is calculated from measured DC I–V and distance between traps are output of PF–model. (d) Activation energy (E_a) and Trap density (N_t) were also extracted from PF–model.

contained a short range of tetrahedral units of GeS, homopolar Ge–Ge or S–S, lone pair, and vacancies [38,39]. This amorphous phase is suitable to modulate conductive channels from the local formation of 'metavalenet' bonds, which is an observable feature of tunable transition between localized and delocalized states [40,41].

3.2. DC electrical characterization

The DC I–V characteristics of the selector devices based on 15–nm–thick $Ge_{1-x}S_x$ films were measured with a voltage sweep of 0.1–V intervals and current compliance at 100 μA. To initiate the device to contain OTS behavior, a higher voltage than V_{th} was applied in the first sweep, called as firing process. In Fig. 2a, devices with Ge–rich compositions ($0.2 \le x < 0.5$) showed permanently reversible metallic behavior after the firing process. This behavior is due to crystallization caused from joule heating during the firing process. *In–situ* XRD measurement at 300 °C was performed to confirm crystallization in firing process. Fig. S2 shows the XRD patterns of $Ge_{1-x}S_x$ films, indicating that Ge–rich films showed sharp peaks corresponding to Ge (111), (220), (311), respectively [42]. Ge–rich films easily formed crystal structures compared with S–rich films because of the Ge contents being higher than the stoichiometry of GeS. On the other hand, devices with S–rich compositions ($0.5 \le x \le 0.67$) demonstrated OTS behaviors with superior performances (V_{th} of 5.0 V and I_{off} of 1.3 nA). To compare electrical performances, V_{th} and I_{off} of previous studies [23,43–46] and those of our work are shown in Fig. 2b. $Si_{1-x}Te_x$ devices showed I_{off} range of 500–390 nA with V_{th} of 1.55 and 1.2 V as the Te increased. In the case of $Ge_{1-x}Te_x$ devices, device based on $GeTe_4$ showed V_{th} of 1.55 V and I_{off} of 200 nA, whereas the device based on $GeTe_6$ exhibited a V_{th} of 1.2 V and lowered I_{off} of 20 nA. Devices based on $Ge_{1-x}Se_x$, V_{th} increased from 4.2 to 4.8 V and I_{off} decreased from 100 to 10 nA as Se contents increased. To enhance the electrical performance of GeSe, As and Bi are doped into GeSe. However, I_{off} still showed 10 and 12 nA for As:GeSe and Bi:GeSe, respectively. On the other hand, our research exhibited a significant decrease in I_{off} as the composition of S increased. I_{off} decreased from 20 to 1.3 nA, whereas V_{th} increased from 3.4 to 5.0 V. The optical bandgap of the $Ge_{1-x}S_x$ films is expected to increase as S increases, which will be discussed in more detail in Fig. 5. It can be estimated that the devices with higher bandgap have a higher V_{th} and lower I_{off}. To understand OTS characteristics of each composition in detail, we investigated key parameters including subthreshold slope (*STS*), inter–trap distance (Δz), activation energy (E_a), and trap density (N_t). The inter–trap distance (Δz) can be calculated using the *STS* equation as follows.

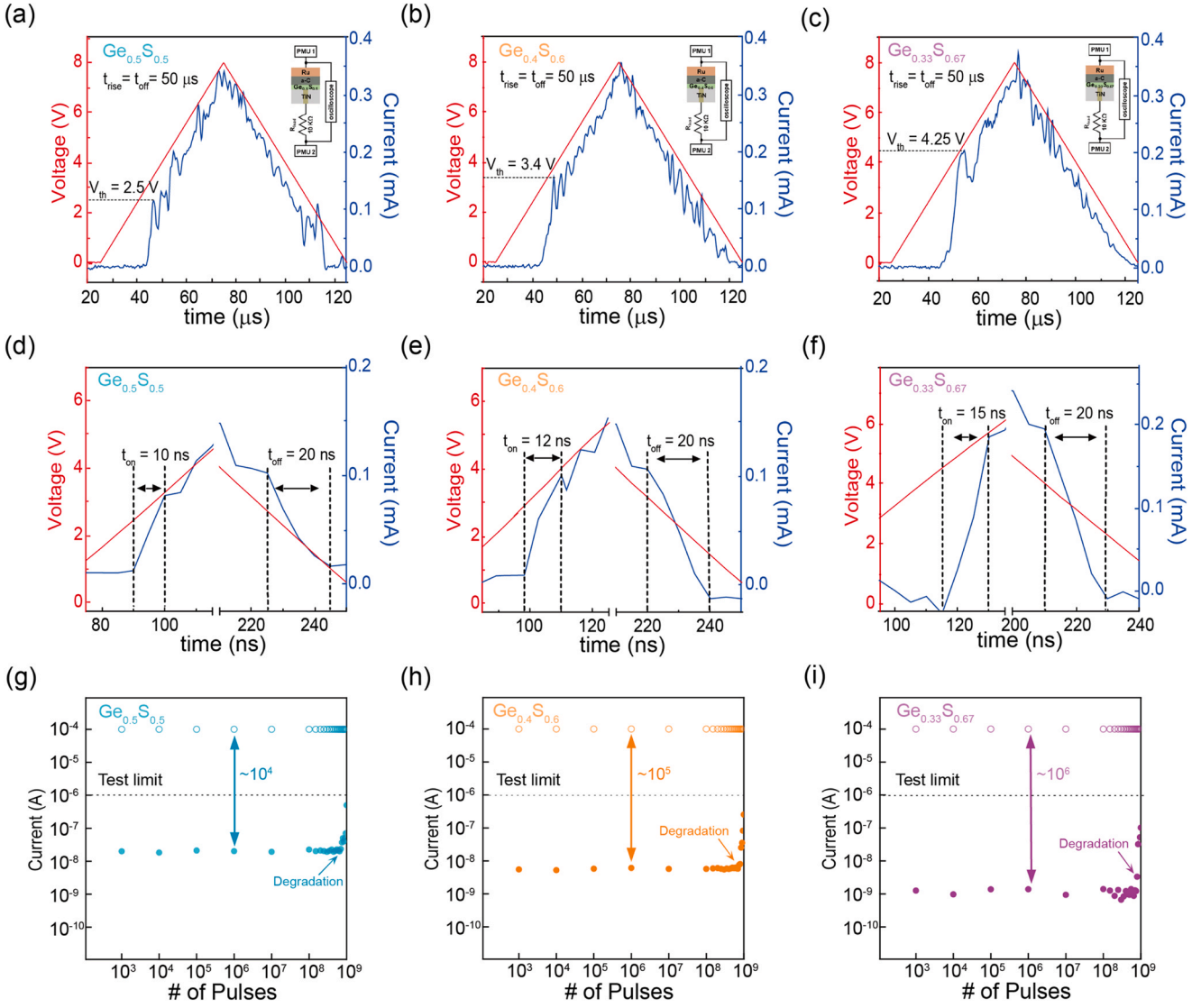

Fig. 3. AC characteristics of the S–rich $G_{1-x}S_x$ devices ($0.5 \le x \le 0.67$) with thicknesses of 15 nm under triangular pulse height of 8 V with different rising/falling time of (a–c) 50 μs and (d–f) 50 ns, respectively. (g–i) Endurance capability of S–rich devices maintaining stable on and off state.

$$STS = \frac{\partial logI}{\partial V_A} = \frac{q}{kT}\frac{\Delta z}{2U_a} \quad (1)$$

where V_A is the applied voltage q is the electric charge k is the Boltzmann constant T is the temperature, and U_a is the thickness of the amorphous film [47]. *STS* can be calculated using the measured I–V curve of $Ge_{0.5}S_{0.5}$, $Ge_{0.4}S_{0.6}$, and $Ge_{0.33}S_{0.67}$ with 15–nm–thick with a range of 0.3 V_{th} to 0.7 V_{th}. As shown in Fig. 2c, *STS* decreased from 1.9068 to 1.5481 as the composition of S increased. Furthermore, Δz was also decreased from 1.5 to 1.2 nm in the same composition range. Trap density is inversely proportional to Δz^3. To extract accurate E_a and N_t, the I–V curves of the S–rich devices were fitted to a PF equation, which can be expressed as

$$I = 2qAN_t\frac{\Delta z}{\tau_0}e^{-(E_C-E_F)/kT}\sinh\left(\frac{qV_A}{kT}\frac{\Delta z}{2U_a}\right) \quad (2)$$

where A is the contact area of the device N_t is the effective trap density, τ_0 is the attempt–to–escape time for the trapped electron, and E_C–E_F is the activation energy. N_t can be calculated using formula $1 / (\Delta z)^3$, τ_0 can be estimated to be 10^{-15} s, and E_C–E_F is the fitting parameter derived from Eq. (2). Substituting parameters from the above formula, activation energies were 0.518, 0.574 and 0.630 eV, whereas N_t were 3.0×10^{20}, 4.6×10^{20} and 5.8×10^{20} cm^{-3} for $Ge_{0.5}S_{0.5}$, $Ge_{0.4}S_{0.6}$, and $Ge_{0.33}S_{0.67}$, respectively. The red lines in Fig. 2a are the calculated I–V by the PF model, which indicated good agreement with the measured I–V curves. These results are consistent with those of other studies on Ge–based binary selectors, $Ge_{1-x}Se_x$ and $Ge_{1-x}Te_x$ [44,48]. The increase in V_{th} and decrease in I_{off} can be attributed to the easy formation of valence alternative pairs in $Ge_{1-x}S_x$ films [49].

3.3. AC electrical characterization

Fig. 3 shows the AC characteristics of S–rich composition devices. A 10 kΩ load resistor was connected in series to prevent overflow of current with compliance of 100 μA. Fig. 3a–c exhibit transient responses of threshold switching with triangular pulse height of 8 V and rising/falling time of 50 μs. At $V_A < V_{th}$, devices remained in highly resistive states with low currents. Then, when $V_A > V_{th}$, the currents increased significantly, indicating V_{th} of 2.5, 3.4, and 4.25 V for devices based on $Ge_{0.5}S_{0.5}$, $Ge_{0.4}S_{0.6}$, and $Ge_{0.33}S_{0.67}$ compositions, respectively. Fig. 3d–f indicates the switching speeds (t_{on}/t_{off}) of the devices. From the same set–up as Fig. 3a–c, only rising/falling time was adjusted to 50 ns. A fast t_{on} of 10, 12, 15 ns for devices based on $Ge_{0.5}S_{0.5}$, $Ge_{0.4}S_{0.6}$, and $Ge_{0.33}S_{0.67}$ films, respectively can be attributed to the OTS phenomenon, which does not require any structural change or atomic rearrangement [50,51]. It is assumed that the higher V_{th} with trap density led to take more time to form a conductive path. In the case of t_{off}, all devices demonstrated a significant decrease with a t_{off} of 20 ns. Those results are fair considering the threshold switching in chalcogenide glasses, which are commonly formed within nanoseconds [52]. AC pulses were applied up to 10^9 cycles to investigate the lifetime of the devices as shown in Fig. 3g–i. After 7.5×10^8 cycles, the I_{off} of the $Ge_{0.5}S_{0.5}$ device began to increase, which indicates that the device degraded. $Ge_{0.4}S_{0.6}$ and $Ge_{0.33}S_{0.67}$ devices maintained a stable on/off state up to 8.5×10^8 cycles. Govoreanu et al. used the TiN top and bottom electrodes to fabricate Ge_xSe_{1-x} devices. Those devices remained in a stable on/off state for ~10^8 cycles [53]. Koo et al. showed SiTe selector using W top and bottom electrodes. This device showed AC endurance up to ~10^8 cycles [54]. This improved stability close to 10^9 cycles, as shown in Fig. 3g–i compared with binary Te/Se based selectors can also be attributed to stronger bonding strength, which allows for the replacement of conventional binary OTS selectors [53–55].

3.4. Thermal stability

Fig. 4a demonstrates the DC I–V curves of S–rich composition devices after baking at 600 °C for 30 min in ambient air to confirm OTS behavior. Even after baking at 600 °C, devices with S–rich compositions retained I–V characteristics with V_{th} of 3.5, 4.1, and 5.2 V for $Ge_{0.5}S_{0.5}$, $Ge_{0.4}S_{0.6}$, and $Ge_{0.33}S_{0.67}$, respectively. ΔV_{th} only varied from 0.1 to 0.2 V compared with the I–V characteristics before baking. This superior thermal stability can be explained by the atomic size difference of Ge and S. The difference in atomic size

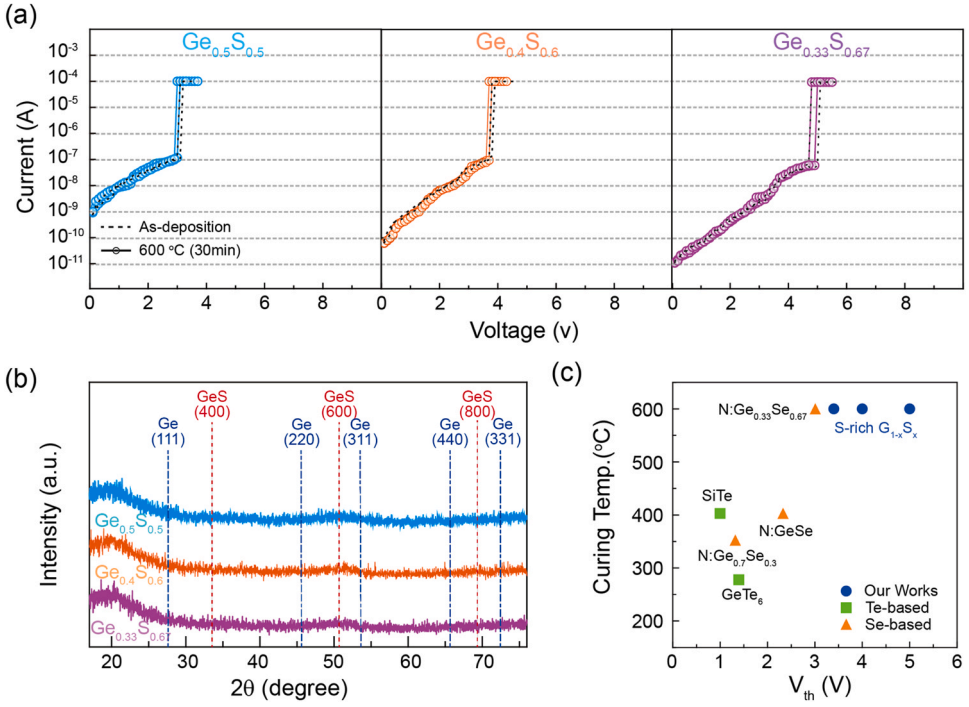

Fig. 4. (a) DC I–V characteristics of S–rich ($0.5 \le x \le 0.67$) devices baked at 600 °C for 30 min. The switching behavior of S–rich devices after baked was similar with the device as deposition. (b) *in–situ* XRD curve of S–rich device after annealing at 600 °C. The S–rich devices are amorphous state after baked. (c) Comparison of thermal stability based on Te/Se selector devices with our work [44,54–56].

increases the energy required for crystallization, which stabilizes the amorphous state. Therefore, a relatively small atomic radius of S (1.09 Å) can suppress crystallization and Ge segregation when bonded with a relatively large atomic radius of Ge (1.52 Å) [27,28]. The smallest covalent radius of S compared with those of other chalcogenides (S 1.05 Å, Se 1.20 Å, and Te 1.38 Å) can result in higher bonding strength when bonded with Ge [29]. *In–xitu* XRD analyses at 600 °C were performed to confirm our argument as shown in Fig. 3b. We deposited 50–nm–thick $Ge_{1-x}S_x$ films with high S contents on a 100–nm–thick SiO_2/Si(P^+) substrate. Fig. 4b confirmed that the amorphous structure was retained up to 600 °C without any segregation and crystallization. To discuss the thermal stability of S–rich of $Ge_{1-x}S_x$ films, the crystallization temperature of other chalcogenide–based OTS selectors is demonstrated in Fig. 4c. Te–based selectors showed poor thermal stability, where $GeTe_6$ [44] showed crystal formation at 275 °C and SiTe can only maintain amorphous structure up to 400 °C [54]. In the case of Se–based selectors with N doping, thermal stability increased as Se contents increased. However, to retain an amorphous state at high temperatures, a complex process is required [55,56]. Our study demonstrates that the smallest covalent radius of S enhances thermal stability when bonded with Ge, which can remain amorphous state above 600 °C without any doping or incorporation.

3.5. Optical properties

To understand the optical characteristics of $Ge_{1-x}S_x$ films, reflectance and transmittance were measured using UV–VIS–NIR Spectroscopy. Applying Beer–Lambert law of light intensity, $T = (1 - R)e^{-\alpha d}$, absorption coefficient (α) can be obtained from reflectance (R), transmittance (T), and thickness (d) [57]. The thicknesses of the layers were fixed at 500 nm on quartz substrates. Reflectance and transmittance were measured with wavelength (λ) ranging from 200 to 2000 nm as shown in Fig. 5–b. The absorption coefficient (α) is determined as follows:

$$\alpha(\lambda) = \frac{1}{d}\ln\frac{1 - R(\lambda)}{T(\lambda)} \quad (1)$$

Fig. 5c shows the tauc plot of $Ge_{1-x}S_x$ films. To calculate optical bandgap, we plotted a graph of $(\alpha h\nu)^n$ versus $h\nu$, where $h\nu$ is the photon energy and n is the nature of the transition. Considering the indirect bandgap of $Ge_{1-x}S_x$ films, n was set to ½ [58]. Each plot was

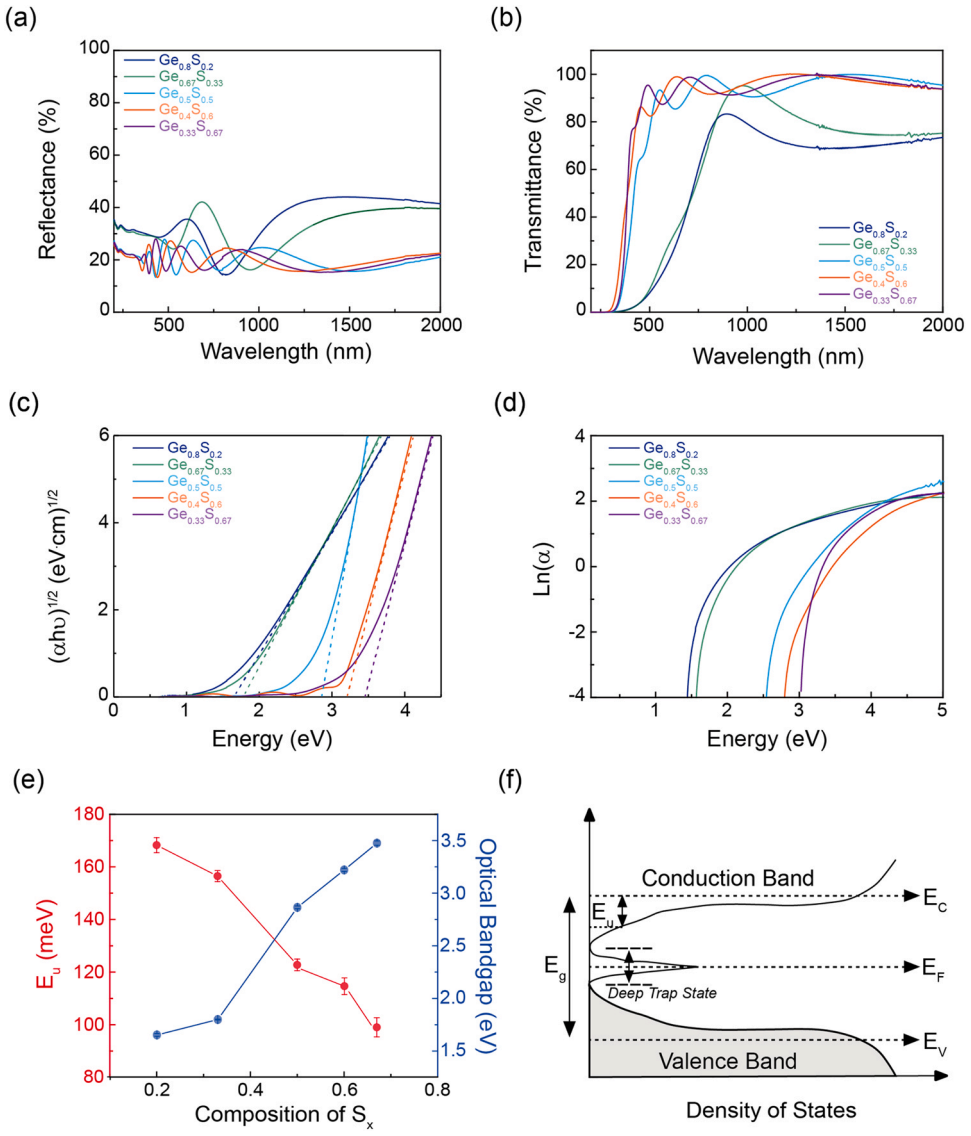

Fig. 5. Optical properties of $Ge_{1-x}S_x$ films deposited on quartz substrate with 500 nm thicknesses: (a) reflectance; (b) transmittance; (c) [$\alpha h\nu$]^0.5 versus photon energy for bandgap extraction; (d) [$Ln(\alpha)$] for urbach energy extraction. (e) Comparison of E_g and E_u as a function of sulfur concentration. (f) Schematic band diagram of $Ge_{1-x}S_x$ films demonstrating locations of E_g, E_u and deep trap state.

fitted linearly, then determined to be 1.65, 1.79, 2.85, 3.21, and 3.45 eV for $Ge_{0.8}S_{0.2}$, $Ge_{0.67}S_{0.33}$, $Ge_{0.5}S_{0.5}$, $Ge_{0.4}S_{0.6}$ and, $Ge_{0.33}S_{0.67}$, respectively. Tanaka et al. calculated the bandgap of GeS_2 as ~3.45 eV. They are well–matched with our data within experimental uncertainty [59]. Considering the well–known bandgaps of Ge (~0.67 eV) and S (~3.8 eV) at room temperature, the bandgap of $Ge_{1-x}S_x$ films is expected to increase as the S content increases [60,61]. Fig. 5d shows fitted urbach energy, the width of defect bands formed near the edge of the bandgap, as follows

$$\alpha = \alpha_0 \exp\left(\frac{E}{E_u}\right) \quad (2)$$

where urbach energy (E_u) can be extracted using 1/slope from the ln (α) versus $h\nu$ graph. Then, E_u of $Ge_{1-x}S_x$ films was calculated to be 166, 159, 122, 115, and 103 meV for $Ge_{0.8}S_{0.2}$, $Ge_{0.67}S_{0.33}$, $Ge_{0.5}S_{0.5}$, $Ge_{0.4}S_{0.6}$, and $Ge_{0.33}S_{0.67}$, respectively, which is closely related to Mott and Davis's model of disordered materials [62]. Urbach energy is affected by the combination of stoichiometry and optical bandgap. As deviated from the stoichiometric composition of $Ge_{1-x}S_x$ layers, the degree of disorder can be increased along with defect formations [59]. Furthermore, urbach energy is inversely proportional to the bandgap, showing that a narrower bandgap is expected to have a wider band tail [63]. Thus, the E_u of $Ge_{0.4}S_{0.6}$ film was lower than that of $Ge_{0.5}S_{0.5}$ film due to a higher bandgap, despite having non-stoichiometric composition.

4. Conclusion

We investigated broad ranges of $Ge_{1-x}S_x$ films to examine OTS behavior, electrical characteristics, and optical properties. Devices with Ge–rich compositions ($0.2 \le x < 0.5$) showed metallic behavior due to Ge crystallization caused by joule heating. On the other hand, devices with S–rich compositions ($0.5 \le x \le 0.67$) indicated superior OTS characteristics and thermal stability. After a firing process, V_{th} increased from 3.4 to 5.0 V and I_{off} decreased from 20 to 1.3 nA as S content increased. The high thermal stability up to 600 °C was verified for both DC I–V characteristics and *in–situ* XRD measurements. Fast on/off of S–rich devices was demonstrated up to 15 ns (t_{on}) and 20 ns (t_{off}) with high stability (~ 10^9 cycles). The optical properties were well–matched with electrical characteristics, indicating films with higher bandgap showed higher V_{th}. Additionally, the optical bandgap of GeS_2 from previous work had good accordance with our calculated bandgap. From this work, we can provide a simple process in 3D stacking arrays and insight into further chalcogenide–based material design, in which bonding strength is deeply contributed to the device performance and stability.

CrediT authorship contribution statement

Minkyu Lee: Conceptualization, Methodology, Validation, Formal analysis, Investigation, Resources, Data curation, Writing – original draft, Writing – review & editing. **Sanghyeon Lee**: Conceptualization, Methodology, Validation, Formal analysis, Investigation, Resources, Data curation, Writing – original draft, Writing – review & editing. **Myoungsub Kim**: Methodology, Validation, Writing – original draft, Formal analysis. **Seungmin Lee**: Validation, Formal analysis, Investigation. **Chihyeong Won**: Resources, Data curation. **Taehoon Kim**: Investigation, Funding acquisition. **Chaebeen Kwon**: Formal analysis. **Kukro Yoon**, **Jinhan Lee**: Data curation. **Hyungjun Kim**: Data curation. **Taeyoon Lee**: Supervision, Project administration, Funding acquisition.

Data availability

The data that has been used is confidential.

Declaration of Competing Interest

The authors declare that they have no known competing financial interests or personal relationships that could have appeared to influence the work reported in this paper.

Acknowledgements

This paper was result of the research project supported by SK hynix Inc. This research was also supported by the Korea Initiative for fostering the University of Research and Innovation (KIURI) Program of the National Research Foundation (NRF) funded by the Korean government (MSIT) (NRF-2020M3H1A1077207), and ICONS (Institute of Convergence Science), Yonsei University. This work was supported by the Korea Medical Device Development Fund grant funded by the Korea government (the Ministry of Science and ICT) (Project Number: KMDF_PR_20200901_0093, 9991006766), and Priority Research Centers Program through the National Research Foundation of Korea (NRF-2019R1A6A1A11055660).

Appendix A. Supporting information

Supplementary data associated with this article can be found in the online version at doi:10.1016/j.jallcom.2022.167409.

References

[1] A. Chung, J. Deen, J.S. Lee, M. Meyyappan, Topical review nanoscale memory devices, Nanotechnology 21 (2010), https://doi.org/10.1088/0957-4484/21/41/412001
[2] A. Sebastian, M. Le Gallo, R. Khaddam-Aljameh, E. Eleftheriou, Memory devices and applications for in-memory computing, Nat. Nanotechnol. 15 (2020) 529–544, https://doi.org/10.1038/s41565-020-0655-z
[3] Z.J. Horváth, B. Horváth, Nanocrystal non-volatile memory devices, Mater. Sci. Forum 609 (2009) 1–9, https://doi.org/10.4028/3-908454-02-6
[4] I.V. Karpov, M. Mitra, D. Kau, G. Spadini, Y.A. Kryukov, V.G. Karpov, Fundamental drift of parameters in chalcogenide phase change memory, J. Appl. Phys. 102 (2007), https://doi.org/10.1063/1.2825650
[5] T. Zhang, Z. Song, B. Liu, S. Feng, B. Chen, Investigation of phase change Si2Sb2Te5 material and its application in chalcogenide random access memory, Solid. State Electron. 51 (2007) 950–954, https://doi.org/10.1016/j.sse.2007.03.016
[6] Y. Yin, H. Sone, S. Hosaka, Simulation of proposed confined-chalcogenide phase-change random access memory for low reset current by finite element modelling, Jpn. J. Appl. Phys., Part 1 Regul. Pap. Short. Notes Rev. Pap. 45 (2006) 6177–6181, https://doi.org/10.1143/JJAP.45.6177
[7] T. Kim, H. Choi, M. Kim, J. Yi, D. Kim, S. Cho, H. Lee, C. Hwang, E.R. Hwang, J. Song, S. Chae, Y. Chun, J.K. Kim, High-performance, cost-effective 2z nm two-deck cross-point memory integrated by self-align scheme for 128 Gb SCM, 37.1.1-37.1.4, Tech. Dig. - Int. Electron Devices Meet. Iedm. 2018-Decem (2019), https://doi.org/10.1109/IEDM.2018.8614680
[8] G.W. Burr, R.S. Shenoy, K. Virwani, P. Narayanan, A. Padilla, B. Kurdi, H. Hwang, Access devices for 3D crosspoint memory, J. Vac. Sci. Technol. B, Nanotechnol. Microelectron. Mater. Process. Meas. Phenom. 32 (2014) 040802, https://doi.org/10.1116/1.4889999
[9] S. Yu, H.Y. Chen, B. Gao, J. Kang, H.S.P. Wong, HfOx-based vertical resistive switching random access memory suitable for bit-cost-effective three-dimensional cross-point architecture, ACS Nano 7 (2013) 2320–2325, https://doi.org/10.1021/nn305510u
[10] J.H. Sung, J.H. Park, D.S. Jeon, D. Kim, M.J. Yu, A.C. Khot, T.D. Dongale, T.G. Kim, Retention enhancement through capacitance-dependent voltage division analysis in 3D stackable TaOx/HfO2-based selectorless memristor, Mater. Des. 207 (2021) 109845, https://doi.org/10.1016/j.matdes.2021.109845
[11] D. Kau, S. Tang, I.V. Karpov, R. Dodge, B. Klehn, J.A. Kalb, J. Strand, A. Diaz, N. Leung, J. Wu, S. Lee, T. Langtry, K.W. Chang, C. Papagianni, J. Lee, J. Hirst, S. Erra, E. Flores, N. Righos, H. Castro, G. Spadini, A stackable cross point phase change memory, Tech. Dig. - Int. Electron Devices Meet. IEDM (2009) 617–620, https://doi.org/10.1109/IEDM.2009.5424263
[12] S. Kim, J. Zhou, W.D. Lu, Crossbar RRAM arrays: selector device requirements during write operation, IEEE Trans. Electron Devices 61 (2014) 2820–2826, https://doi.org/10.1109/TED.2014.2327514
[13] D. Kim, J.H. Park, D.S. Jeon, T.D. Dongale, T.G. Kim, Ta2O5-y-based ReRAM device with annealing-free Ag:ZrNx-based bilayer selector device, J. Alloy. Compd. 854 (2021) 157261, https://doi.org/10.1016/j.jallcom.2020.157261
[14] T.D. Dongale, G.U. Kamble, D.Y. Kang, S.S. Kundale, H. An, T.G. Kim, Recent Progress in Selector and Self-Rectifying Devices for Resistive Random-Access Memory Application, 2100199 (2021) 1–22. https://doi.org/10.1002/pssr.202100199.

[15] D.S. Jeon, T.D. Dongale, T.G. Kim, Low power Ti-doped NbO2-based selector device with high selectivity and low OFF current, J. Alloy. Compd. 884 (2021) 161041, https://doi.org/10.1016/j.jallcom.2021.161041

[16] S.R. Ovshinsky, Reversible electrical switching phenomena in disordered structures, Phys. Rev. Lett. 21 (1968) 1450–1453, https://doi.org/10.1103/PhysRevLett.21.1450

[17] H. Li, W. Chen, First-principles prediction of the native filament:dielectric interfaces for the possible filamentary switching mechanism in chalcogenide selector devices, J. Appl. Phys. 127 (2020), https://doi.org/10.1063/1.5134916

[18] H. Li, J. Robertson, Materials selection and mechanism of non-linear conduction in chalcogenide selector devices, Sci. Rep. 9 (2019) 1–9, https://doi.org/10.1038/s41598-018-37717-x

[19] M.J. Yu, K.R. Son, A.C. Khot, D.Y. Kang, J.H. Sung, I.G. Jang, Y.D. Dange, T.D. Dongale, T.G. Kim, Three Musketeers: demonstration of multilevel memory, selector, and synaptic behaviors from an Ag-GeTe based chalcogenide material, J. Mater. Res. Technol. 15 (2021) 1984–1995, https://doi.org/10.1016/j.jmrt.2021.09.044

[20] M. Anbarasu, M. Wimmer, G. Bruns, M. Salinga, M. Wuttig, Nanosecond threshold switching of GeTe 6 cells and their potential as selector devices, Appl. Phys. Lett. 100 (2012), https://doi.org/10.1063/1.3700743

[21] B. Song, H. Xu, S. Liu, H. Liu, Q. Liu, Q. Li, An ovonic threshold switching selector based on Se-rich GeSe chalcogenide, Appl. Phys. A Mater. Sci. Process. 125 (2019) 1–6, https://doi.org/10.1007/s00339-019-3073-z

[22] S.A. Chekol, J. Yoo, J. Park, J. Song, C. Sung, H. Hwang, A. C-Te-based, binary OTS device exhibiting excellent performance and high thermal stability for selector application, Nanotechnology 29 (2018), https://doi.org/10.1088/1361-6528/aac9f5

[23] A. Verdy, G. Navarro, V. Sousa, P. Noé, M. Bernard, F. Fillot, G. Bourgeois, J. Garrione, L. Perniola, Improved electrical performance thanks to Sb and N Doping in Se-rich GeSe-Based OTS selector devices, 2017 IEEE 9th Int. Mem. Work. IMW 2017 (2017) 8–11, https://doi.org/10.1109/IMW.2017.7939088

[24] G. Liu, T. Li, L. Wu, Y. Chen, B. Liu, Z. Ma, S. Song, Z. Song, Increasing trapped carrier density in nanoscale GeSeAs films by As ion implantation for selector devices in 3D-stacking memory, ACS Appl. Nano Mater. 2 (2019) 5373–5380, https://doi.org/10.1021/acsanm.9b00734

[25] S. Jia, H. Li, T. Gotoh, C. Longeaud, B. Zhang, J. Lyu, S. Lv, M. Zhu, Z. Song, Q. Liu, J. Robertson, M. Liu, Ultrahigh drive current and large selectivity in GeS selector, Nat. Commun. 11 (2020) 1–9, https://doi.org/10.1038/s41467-020-18382-z

[26] M. Kim, Y. Kim, M. Lee, S.M. Hong, H.K. Kim, S. Yoo, T. Kim, S.M. Chung, T. Lee, H. Kim, PE-ALD of Ge1−xSxamorphous chalcogenide alloys for OTS applications, J. Mater. Chem. C. 9 (2021) 6006–6013, https://doi.org/10.1039/d1tc00650a

[27] Y.S. Yun, H.S. Nam, P.R. Cha, W.T. Kim, D.H. Kim, Effects of atomic size difference and heat of mixing parameters on the local structure of a model metallic glass system, Met. Mater. Int. 20 (2014) 105–111, https://doi.org/10.1007/s12540-013-6013-z

[28] H.S. Chen, Thermodynamic considerations on the formation and stability of metallic glasses, Acta Met. 22 (1974) 1505–1511, https://doi.org/10.1016/0001-6160(74)90112-6

[29] A. Bytchkov, G.J. Cuello, S. Kohara, C.J. Benmore, D.L. Price, E. Bychkov, Unraveling the atomic structure of Ge-rich sulfide glasses, Phys. Chem. Chem. Phys. 15 (2013) 8487–8494, https://doi.org/10.1039/c3cp50536g

[30] A.C. Galca, F. Sava, I.D. Simandan, C. Bucur, V. Dumitru, C. Porosnicu, C. Mihai, A. Velea, Structural and optical properties of optimized amorphous GeTe films for memory applications, J. Non Cryst. Solids 499 (2018) 1–7, https://doi.org/10.1016/j.jnoncrysol.2018.07.007

[31] H. Zhao, Y. Mao, X. Mao, X. Shi, C. Xu, C. Wang, S. Zhang, D. Zhou, Band structure and photoelectric characterization of GeSe monolayers, Adv. Funct. Mater. 28 (2018) 1–10, https://doi.org/10.1002/adfm.201704855

[32] C.C. Wu, C.H. Ho, J.Y. Wu, S.L. Lin, Y.S. Huang, Characterization of Ge(Se1-xSx)2 series layered crystals grown by vertical Bridgman method, J. Cryst. Growth 281 (2005) 377–383, https://doi.org/10.1016/j.jcrysgro.2005.04.001

[33] Y. Yang, S.C. Liu, X. Wang, Z. Li, Y. Zhang, G. Zhang, D.J. Xue, J.S. Hu, Polarization-sensitive ultraviolet photodetection of anisotropic 2D GeS 2, Adv. Funct. Mater. 29 (2019) 1–6, https://doi.org/10.1002/adfm.201900411

[34] B.A. Hasan, M.A. Kadhim, Effect of germanium content on the optical constants of GexS1-xThin films, IOP Conf. Ser. Mater. Sci. Eng. 928 (2020), https://doi.org/10.1088/1757-899X/928/7/072009

[35] M.C. Cyrille, A. Verdy, G. Navarro, G. Bourgeois, J. Garrione, M. Bernard, C. Sabbione, P. Noe, E. Nowak, OTS selector devices: Material engineering for switching performance, ICICDT 2018 - Int. Conf. IC Des. Technol. Proc. (2018) 113–116. https://doi.org/10.1109/ICICDT.2018.8399769.

[36] A. Verdy, G. Navarro, M. Bernard, S. Chevalliez, N. Castellani, E. Nolot, J. Garrione, P. Noe, G. Bourgeois, V. Sousa, M.C. Cyrille, E. Nowak, Carbon electrode for Ge-Se-Sb based OTS selector for ultra low leakage current and outstanding endurance, IEEE Int. Reliab. Phys. Symp. Proc. 2018-March (2018) 6D.41–6D.46. https://doi.org/10.1109/IRPS.2018.8353635.

[37] M.S. Seo, S.W. Lee, Arsenic-free ovonic threshold switch for next-generation selectors in 3-dimensional cross-point memories, Mater. Today Commun. 29 (2021) 102849, https://doi.org/10.1016/j.mtcomm.2021.102849

[38] J. Heo, J.M. Yoon, S.Y. Ryou, Raman spectroscopic analysis on the solubility mechanism of La3+ in GeS2-Ga2S3 glasses, J. Non Cryst. Solids 238 (1998) 115–123, https://doi.org/10.1016/S0022-3093(98)00577-8

[39] S. Sen, C.W. Ponader, B.G. Aitken, Ge and As x-ray absorption fine structure spectroscopic study of homopolar bonding, chemical order, and topology in Ge-As-S chalcogenide glasses, Phys. Rev. B - Condens. Matter Mater. Phys. 64 (2001) 1–10, https://doi.org/10.1103/PhysRevB.64.104202

[40] B.J. Kooi, M. Wuttig, Chalcogenides by design: functionality through metavalent bonding and confinement, Adv. Mater. 32 (2020), https://doi.org/10.1002/adma.201908302

[41] M. Zhu, O. Cojocaru-Mirédin, A.M. Mio, J. Keutgen, M. Küpers, Y. Yu, J.Y. Cho, R. Dronskowski, M. Wuttig, Unique bond breaking in crystalline phase change materials and the quest for metavalent bonding, Adv. Mater. 30 (2018), https://doi.org/10.1002/adma.201706735

[42] E. Hüger, F. Strauß, J. Stahn, J. Deubener, M. Bruns, H. Schmidt, In-situ measurement of self-atom diffusion in solids using amorphous germanium as a model system, Sci. Rep. 8 (2018) 1–8, https://doi.org/10.1038/s41598-018-35915-1

[43] J. Seo, H.W. Ahn, S.Y. Shin, B.K. Cheong, S. Lee, Anomalous reduction of the switching voltage of Bi-doped Ge 0.5Se0.5 ovonic threshold switching devices, Appl. Phys. Lett. 104 (2014) 3–7, https://doi.org/10.1063/1.4871385

[44] A. Velea, K. Opsomer, W. Devulder, J. Dumortier, J. Fan, C. Detavernier, M. Jurczak, B. Govoreanu, Te-based chalcogenide materials for selector applications, Sci. Rep. 7 (2017) 1–12, https://doi.org/10.1038/s41598-017-08251-z

[45] H.Y. Cheng, W.C. Chien, I.T. Kuo, C.W. Yeh, L. Gignac, W. Kim, E.K. Lai, Y.F. Lin, R.L. Bruce, C. Lavoie, C.W. Cheng, A. Ray, F.M. Lee, F. Carta, C.H. Yang, M.H. Lee, H.Y. Ho, M. Brightsky, H.L. Lung, Ultra-high endurance and low I OFF selector based on AsSeGe chalcogenides for wide memory window 3D stackable cross-point memory, 37.3.1-37.3.4, Tech. Dig. - Int. Electron Devices Meet. Iedm. 2018-Decem (2019), https://doi.org/10.1109/IEDM.2018.8614580

[46] H.W. Ahn, D.S. Jeong, B.K. Cheong, S.D. Kim, S.Y. Shin, H. Lim, D. Kim, S. Lee, A study on the scalability of a selector device using threshold switching in Pt/GeSe/Pt, ECS Solid State Lett. 2 (2013) 31–34, https://doi.org/10.1149/2.011309ssl

[47] D. Ielmini, Y. Zhang, Analytical model for subthreshold conduction and threshold switching in chalcogenide-based memory devices, J. Appl. Phys. 102 (2007), https://doi.org/10.1063/1.2773688

[48] S.D. Kim, H.W. Ahn, S.Y. Shin, D.S. Jeong, S.H. Son, H. Lee, B.K. Cheong, D.W. Shin, S. Lee, Effect of Ge concentration in GeXse1-x chalcogenide glass on the electronic structures and the characteristics of ovonic threshold switching (OTS) devices, ECS Solid State Lett. 2 (2013) 75–77, https://doi.org/10.1149/2.001310ssl

[49] M. Kastner, D. Adler, H. Fritzsche, Valence-alternation model for localized gap states in lone-pair semiconductors, Phys. Rev. Lett. 37 (1976) 1504–1507, https://doi.org/10.1103/PhysRevLett.37.1504

[50] D. Ielmini, Threshold switching mechanism by high-field energy gain in the hopping transport of chalcogenide glasses, Phys. Rev. B - Condens. Matter Mater. Phys. 78 (2008) 1–8, https://doi.org/10.1103/PhysRevB.78.035308

[51] S.R. Ovshinsky, An introduction to ovonic research, J. Non Cryst. Solids 2 (1970) 99–106, https://doi.org/10.1016/0022-3093(70)90125-0

[52] D. Adler, M.S. Shur, M. Silver, S.R. Ovshinsky, Threshold switching in chalcogenide-glass thin films, J. Appl. Phys. 51 (1980) 3289–3309, https://doi.org/10.1063/1.328036

[53] N.S. Avasarala, A. Redolfi, S. Kundu, O. Richard, D. Tsvetanova, G. Pourtois, C. Detavernier, L. Goux, G.S. Kar, T7–2 T92 T93, 21 (2017) 92–93.

[54] Y. Koo, S. Lee, S. Park, M. Yang, H. Hwang, Simple binary ovonic threshold switching material SiTe and its excellent selector performance for high-density memory array application, IEEE Electron Device Lett. 38 (2017) 568–571, https://doi.org/10.1109/LED.2017.2685435

[55] N.S. Avasarala, G.L. Donadio, T. Witters, K. Opsomer, B. Govoreanu, A. Fantini, S. Clima, H. Oh, S. Kundu, W. Devulder, M.H. Van Der Veen, J. Van Houdt, M. Heyns, L. Goux, G.S. Kar, Half-threshold bias Ioff reduction down to nA range of thermally and electrically stable high-performance integrated OTS selector, obtained by Se enrichment and N-doping of thin GeSe layers, Dig. Tech. Pap. - Symp. VLSI Technol. 2018-June (2018) 209–210. https://doi.org/10.1109/VLSIT.2018.8510680.

[56] J. Keukelier, K. Opsomer, W. Devulder, S. Clima, L. Goux, G. Sankar Kar, C. Detavernier, Tuning of the thermal stability and ovonic threshold switching properties of GeSe with metallic and non-metallic alloying elements, J. Appl. Phys. 130 (2021), https://doi.org/10.1063/5.0055861

[57] S. Cosentino, M. Miritello, I. Crupi, G. Nicotra, F. Simone, C. Spinella, A. Terrasi, S. Mirabella, Room-temperature efficient light detection by amorphous Ge quantum wells, Nanoscale Res. Lett. 8 (2013) 1–7, https://doi.org/10.1186/1556-276X-8-128

[58] D.D. Vaughn, R.J. Patel, M.A. Hickner, R.E. Schaak, Single-crystal colloidal nanosheets of GeS and GeSe, J. Am. Chem. Soc. 132 (2010) 15170–15172, https://doi.org/10.1021/ja107520b

[59] K. Tanaka, Y. Kasanuki, A. Odajima, Physical properties and photoinduced changes of amorphous Ge-S films, Thin Solid Films 117 (1984) 251–260.

[60] P. Liu, P. Longo, A. Zaslavsky, D. Pacifici, Optical bandgap of single- and multi-layered amorphous germanium ultra-thin films, J. Appl. Phys. 119 (2016), https://doi.org/10.1063/1.4939296

[61] R.R. Thankalekshmi, A.C. Rastogi, Structure and optical band gap of ZnO 1-xS x thin films synthesized by chemical spray pyrolysis for application in solar cells, J. Appl. Phys. 112 (2012) 1–10, https://doi.org/10.1063/1.4754014

[62] N.F. Mott, E.A. Davis, Conduction in non-crystalline systems V. Conductivity, optical absorption and photoconductivity in amorphous semiconductors, Philos. Mag. 22 (1970) 903–922, https://doi.org/10.1080/14786437008221061

[63] F.N.C. Anyaegbunam, C. Augustine, A study of optical band gap and associated Urbach energy tail of chemically deposited metal oxides binary thin films, Dig. J. Nanomater. Biostruct. 13 (2018) 847–856 ⟨http://www.chalcogen.ro/847_AugustineC.pdf⟩.